PERGAMON

Micron 31 (2000) 363–372

micron

www.elsevier.com/locate/micron

Understanding STM images and EELS spectra of oxides with strongly correlated electrons: a comparison of nickel and uranium oxides

S.L. Dudarev[a,*], M.R. Castell[a], G.A. Botton[b], S.Y. Savrasov[c], C. Muggelberg[a], G.A.D. Briggs[a], A.P. Sutton[a], D.T. Goddard[d]

[a]*Department of Materials, University of Oxford, Parks Road, Oxford OX1 3PH, UK*
[b]*Materials Technology Laboratory, CANMET, 568 Booth Street, Ottawa, Ont., Canada K1A 0G1*
[c]*Max-Planck-Institut für Festkörperforschung, Heisenbergstraße 1, D-70569 Stuttgart, Germany*
[d]*Research and Technology, BNFL, Springfields Works, Salwick, Preston, Lancashire PR4 0XJ, UK*

Abstract

Using a theoretical approach combining the local spin density approximation (LSDA) of density functional theory and the Hubbard U term (LSDA + U), we analyse the connection between the experimentally observed electron energy loss spectra *and* elevated temperature scanning tunnelling images of surfaces of semiconducting nickel monoxide NiO and uranium dioxide UO_2. We show that a combination of electron energy loss spectroscopy, atomic-resolution tunnelling imaging and first-principles ab initio calculations provides a powerful tool for studying electronic and structural properties of surfaces of transition metal and actinide oxides.

1. Introduction

Sixty years ago in a pioneering paper de Boer and Verwey (1937) drew attention to a class of 'anomalous' insulating transition metal oxides, whose electronic structure could not be described using conventional band theory. The origin of the insulating behaviour of those oxides was unravelled by Peierls and Mott (1937) who pointed out that band theory fails when the inter-site quantum hopping (tunnelling) of electrons is suppressed by the on-site Coulomb repulsion between electrons. In the limiting case where the amplitude of hopping (characterized by the magnitude of the overlap integral t) is comparable or smaller than the Hubbard U term (where U is the energy of repulsion between electrons occupying the same atomic shell), the motion of electrons in a crystal becomes strongly correlated and the compound exhibits properties that do not agree with predictions made using conventional band theory (Adler, 1968). The anomalous transport properties of transition metal oxides studied experimentally by de Boer and Verwey (1937) and discussed theoretically by Peierls and Mott (1937) and Mott (1974) also manifest themselves in other transition metal compounds (e.g. sulphades) and in compounds containing ions of actinide elements. Metal ions in these compounds contain partly filled d- and f-shells where electrons are localized in the vicinity of atomic cores. The strength of Coulomb repulsion between electrons occupying these shells is significantly larger than the strength of Coulomb interaction between electrons in s- and p-type materials.

Despite the fact that the fundamental nature of interactions giving rise to the variety of experimentally observed effects is simple (essentially all of the observed 'anomalies' result from the interplay between the intersite hopping of electrons, the Coulomb interaction between electrons occupying the same or neighbouring sites, and the symmetry of atomic states involved), the problem of developing a consistent mathematical description of properties of transition metal and actinide compounds still represents one of the most challenging tasks in condensed matter physics and materials science. The reason why this is so is described in a brief note by Spalek (1990) and in a number of comprehensive reviews including those by Adler (1968) and by Brandow (1977) and also in a book by Fulde (1995). A thorough account of spectroscopical information on NiO and related compounds is given in a review by Hüfner (1994).

So far, experimental and theoretical studies of transition metal and actinide oxides were mainly focused on their *bulk* properties. This included investigations of transport

* Corresponding author. UKAEA Fusion, D3 Culham Science Centre, Abingdon, Oxfordshire OX14 3DB, UK. Tel.: +44-1235-463513; fax: +44-1235-463435.

E-mail address: sergei.dudarev@ukaea.org.uk (S.L. Dudarev).

0968–4328/00/$ - see front matter
PII: S0968-4328(99)00115-8

properties and superconductivity occurring in some of the oxides, and also studies of effects like colossal magnetoresistance and various other manifestations of interaction between localized magnetic moments.

In our work we concentrate mainly on the *surface* properties of transition metal and actinide oxides. This field has recently attracted attention of many research groups worldwide. The interest in the electronic and structural properties of transition metal and actinide oxide surfaces is primarily driven by applications of these oxides in the field of heterogeneous catalysis. Hutchins et al. (1996) showed that uranium oxides could be used as catalysts for the destruction of volatile chloro-organic compounds. Transition metal oxides exhibit similar catalytic properties (see Gordon et al., 1996) and there is evidence for the existence of a link between strong electron correlations and the catalytic activity of oxide surfaces (Kiselev and Krylov, 1989).

Catalytic behaviour is a complex phenomenon where the activity of a particular oxide depends on the atomic structure of its surfaces and where the selectivity with respect to a particular reaction depends on the type of electronic excitations associated with a particular termination of the surface (Ertl and Freund, 1999). Catalytic activity of oxides also shows dependence on the presence of atomic steps and defects on the surface. Surface energy loss spectroscopy (surface EELS) has recently been used to characterize the electronic structure of an oxide surface at a quantitative level (Freitag et al., 1993; Gorschlüter and Merz, 1994). However, the level of spatial resolution accessible to surface EELS is still too low to permit reliable identification of contributions from individual atomic steps and defects.

One of the novel experimental techniques that combines the sensitivity to the atomic *and* electronic structure of surfaces is scanning tunnelling microscopy (STM), where the observed signal is formed by electrons tunnelling through a narrow vacuum gap between a (metallic) tip and a surface. STM has already been applied with considerable success to atomically resolved imaging of surfaces of metals and doped semiconductors. However, until recently no data have been reported in the literature on the application of STM to the study of surfaces of insulating (at room temperature) transition metal and actinide oxides. Advances that have been made during the last three years in this field are associated with the development of a new approach to tunnelling imaging of surfaces of insulating oxides that involves carrying out observations at elevated temperature (Castell et al., 1997a,b, 1998a,b, 1999; Muggelberg, 1997; Muggelberg et al. 1998a,b). Dudarev et al. (1997a, 1999) showed that to interpret STM images of transition metal and actinide oxides it is necessary to address a number of fundamental issues that have not been investigated in the standard theoretical treatment of tunnelling images developed by Tersoff and Hamann (1985). Among them the most important one concerns the inclusion in a computational method of effects of strong Coulomb repulsion between electrons occupying partly filled d- or f-shells of metal ions. In this paper we show how this can be achieved within the framework of the full-potential LMTO implementation of the LSDA + U method. The LSDA + U method is an approach that combines the local spin density approximation of density functional theory with the Hubbard U term. Below, we discuss applications of LSDA + U to the interpretation of STM images of NiO(001) and UO_2(111) surfaces. We also show how to use the LSDA + U method to model electron energy loss spectra (EELS) of NiO and UO_2 and how to use EELS to determine parameters characterizing the effective strength of Coulomb repulsion between d- or f-electrons in these two oxides.

2. The LSDA + U method

The LSDA + U method was proposed by Anisimov et al. (1991) in order to bridge the gap between ab initio density functional (DFT) methods based on local density approximation (LDA) and many-body approaches to the treatment of strongly correlated electronic systems. While being very successful in a number of cases, conventional DFT-LDA approaches often fail when they are applied to the treatment of *insulating* states of compounds containing partly filled d- and f-shells. For example, in the case of uranium dioxide UO_2 all of the reported applications of DFT-LDA have led to the prediction of a metallic ground state despite the fact that experimentally UO_2 is known to be a good insulator, see e.g. Dudarev et al. (1997b).

The history of applications of LSDA + U to d- and f-electron compounds has been recently reviewed by Anisimov et al. (1997). It is now well understood that LSDA + U represents a convenient way of combining the linear muffin-tin orbital (LMTO) implementation of DFT-LDA (for the description of the full-potential LMTO code used here see papers by Savrasov and Savrasov (1992) and Savrasov (1996)), with the unrestricted Hartree–Fock (UHF) treatment of effects of on-site repulsion between electrons (Fradkin, 1991).

To describe the Coulomb interaction between 5f electrons of uranium ions in UO_2 or between 3d electrons of nickel ions in NiO we use a model Hamiltonian of the form (Kotani and Yamazaki, 1992)

$$\hat{H} = \frac{\bar{U}}{2} \sum_{m,m',\sigma} \hat{n}_{m,\sigma}\hat{n}_{m',-\sigma} + \frac{(\hat{U} - \bar{J})}{2} \sum_{m \neq m',\sigma} \hat{n}_{m,\sigma}\hat{n}_{m',\sigma}, \qquad (1)$$

where summation is performed over projections of the orbital momentum ($m, m' = -3, -2 \ldots, 3$ in the case of f-electrons) and $\bar{U}$ and $\bar{J}$ are the spherically averaged matrix elements of the *screened* electron–electron interaction. Hamiltonian (1) is similar to the one used in the original formulation of LDA + U proposed by Anisimov et al. (1991).

Following the derivation given by Dudarev et al. (1998a,b), we arrive at the following equation for the matrix

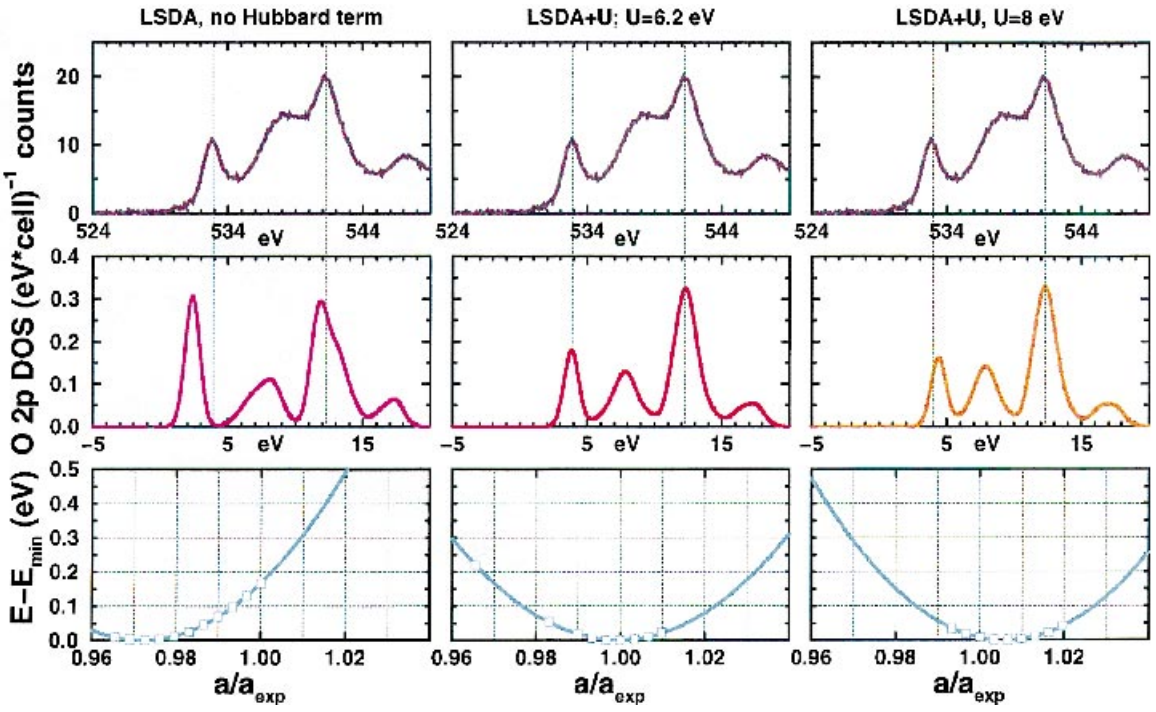

Fig. 1. A graphical illustration of the procedure that was followed to determine the magnitude of the Hubbard $\bar{U}$ for NiO. The upper row shows the experimentally measured oxygen K edge EELS spectrum of NiO. The middle row of graphs shows a series of simulated EELS spectra representing the distribution of the density of empty oxygen 2p states broadened with a 0.5 eV wide gaussian function. The bottom row of graphs shows the total energy of one unit cell of NiO plotted as a function of the lattice parameter. The choice of $\bar{U} = 6.2$ eV and $\bar{J} = 0.95$ eV makes it possible to reproduce well the experimentally observed EELS spectra *and* it also gives rise to the value of the equilibrium lattice constant that is close to the value observed experimentally.

of the effective LSDA + U potential

$$V_{jl}^{\sigma} \equiv \frac{\delta E_{\mathrm{LSDA}+U}}{\delta \rho_{lj}^{\sigma}} = \frac{\delta E_{\mathrm{LSDA}}}{\delta \rho_{lj}^{\sigma}} + (\bar{U} - \bar{J})\left[\frac{1}{2}\delta_{jl} - \rho_{jl}^{\sigma}\right], \quad (2)$$

where ρ_{jl}^{σ} is the density matrix of electrons occupying a partly filled electronic shell (5f in UO_2 and 3d in NiO). The total energy of the solid is expressed in terms of the Kohn–Sham eigenvalues $\{\epsilon_i\}$ as

$$E_{\mathrm{LSDA+U}} = E_{\mathrm{LSDA}}[\{\epsilon_i\}] + \frac{(\bar{U} - \bar{J})}{2} \sum_{l,j,\sigma} \rho_{lj}^{\sigma} \rho_{jl}^{\sigma}, \quad (3)$$

where the last term is added to eliminate double counting of electrons.

The Hubbard correction to the LSDA potential in Eq. (2) affects the dispersion of electronic states and, for a sufficiently large value of $\bar{U}$, it leads to the formation of a band gap in the otherwise metallic spectrum of excitations (Anisimov et al., 1991). The Hubbard correction term also changes the total energy of the solid, Eq. (3), altering the position of the minimum of the total energy functional and affecting the predicted equilibrium structure of the solid. In the case of NiO and UO_2 predictions following from LSDA + U calculations (Dudarev et al., 1998b) agree better with experimental data than results obtained using conventional LSDA.

Summarizing the points described in this section, we would like to emphasize that LSDA + U approach represents an attempt to develop an effective *one-particle* approach to the electronic structure of materials with strongly correlated electrons. The mean-field (or equivalently, the unrestricted Hartree–Fock) approximation on which the LSDA + U approach is based, should be expected to break down in cases where fluctuations of occupation numbers become significant. The treatment of phenomena associated with fluctuating occupation numbers requires going beyond LSDA + U and in recent years significant progress has been made in the development of more mathematically exact approaches to the treatment of electron–electron interactions in real systems (Lichtenstein and Katsnelson, 1998).

3. Electronic structure of NiO and UO_2 and the interpretation of EELS spectra

In this paper we consider applications of LSDA + U to the interpretation of STM images of two oxides: nickel oxide NiO and uranium dioxide UO_2. Why is it necessary to use LSDA + U instead of DFT-LDA to understand tunnelling of electrons at surfaces of these two oxides? NiO represents a classical example of the violation of rules of conventional band theory (De Boer and Verwey, 1937; Adler, 1968). In the absence of magnetic ordering DFT-LDA predicts metallic ground state for NiO, and the situation improves only marginally if antiferromagnetic

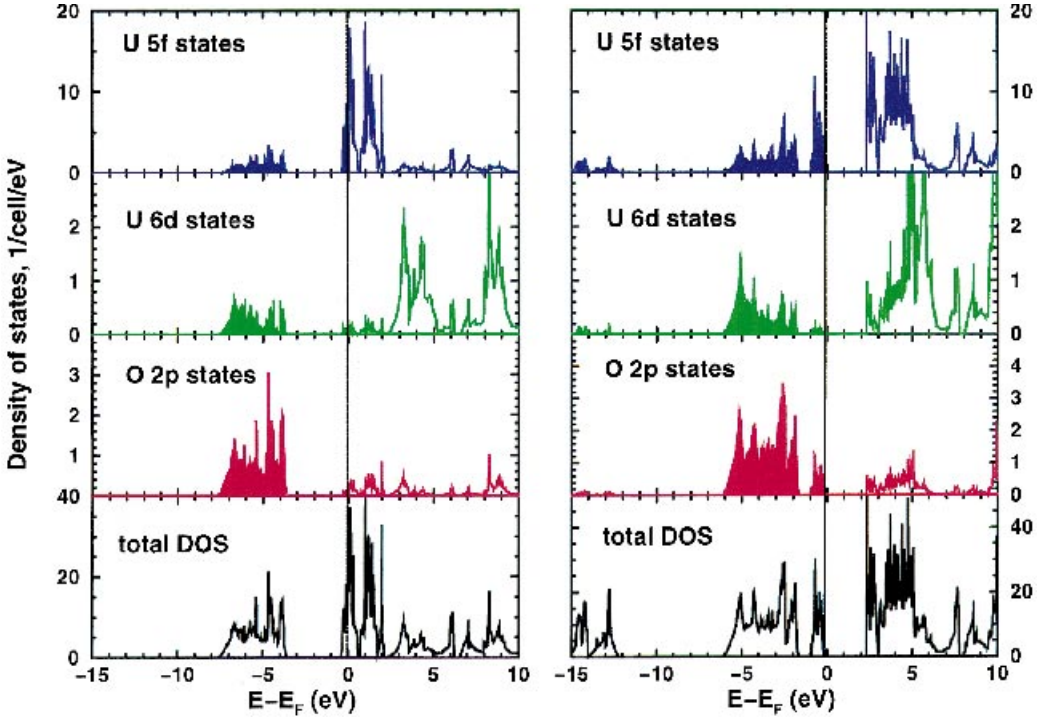

Fig. 2. The density of uranium 5f and 6d states and oxygen 2p state in uranium dioxide. Both the LSDA and LSDA + U calculations were performed assuming the experimentally observed antiferromagnetic ground state. The band gap obtained for $\bar{U} = 4.5$ eV and $\bar{J} = 0.5$ eV equals 2.1 eV.

order is taken into account, see Anisimov et al. (1991). The main deficiency of DFT-LDA calculations is that it predicts that semiconducting NiO is a pure Mott–Hubbard insulator while spectroscopical data (Hüfner, 1994) show that it has a very significant charge transfer character. Moreover, the size of the band gap in NiO following from a DFT-LDA calculation (0.4 eV) is too small in comparison with the band gap observed experimentally (4.3 eV).

In the case of uranium dioxide DFT-LDA calculations lead to the prediction of a metallic ground state even if the experimentally observed type of antiferromagnetic ordering is taken into account (Dudarev et al., 1997b). The band gap in UO_2 observed experimentally is close to 2 eV, and reproducing this value correctly is essential for interpreting the experimentally observed scanning tunnelling images. Therefore, both in the case of NiO and in the case of UO_2 taking the Hubbard $\bar{U}$ term into account is necessary to describe adequately the spectrum of one-electron excitations of the material. In the case of NiO the origin of the observed insulating ground state is associated with the presence of strong Coulomb repulsion between the 3d electrons localized on Ni sites. In the case of UO_2 the insulating nature of the ground state results from the presence of Hubbard correlations in the band of uranium 5f states.

One of the central points of any application of LSDA + U consists in the determination of values of $\bar{U}$ and $\bar{J}$ entering Eqs. (1)–(3). In principle, these two quantities can be evaluated by carrying out a supercell calculation, see Anisimov et al., 1991. However, presently it is known that values of $\bar{U}$ obtained from supercell calculations are not very reliable and in some cases the error in the determination of $\bar{U}$ may be as large as 50% (the value of $\bar{J}$ characterizing individual atoms changes only little when a solid is formed and it is therefore possible to use atomic values of this parameter in calculations, see Anisimov et al., 1993). To determine the value of $\bar{U}$ characterizing the strength of Coulomb repulsion between 3d electrons in NiO and 5f electrons in UO_2 we have therefore followed a different route. Our approach is based on the realization of the fact that, since the LSDA + U method described above contains essentially only one 'adjustable' parameter $\bar{U} - \bar{J}$, see Eqs. (2) and (3), it should be possible to use complementary experimental information to deduce the value of $\bar{U} - \bar{J}$ that matches all the available experimental data in the best possible way. For example, we should expect that if the value of $\bar{U} - \bar{J}$ is chosen adequately then a self-consistent calculation should describe well both the excitation spectra of the compound *and* its equilibrium properties, e.g. its lattice parameter and elastic constants. An illustration of the procedure that we followed for the case of NiO is given in Fig. 1.

To simulate the experimentally observed EELS spectra we evaluated the partial densities of states projected on orbitals of given symmetry localized on various atoms in a unit cell. Fig. 1 shows a comparison of experimentally

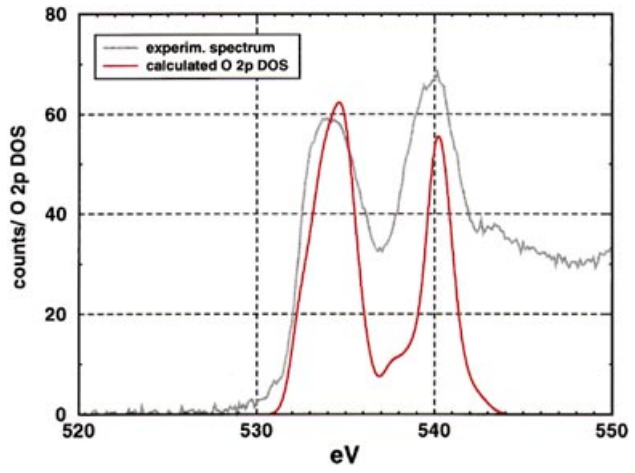

Fig. 3. Electron energy loss spectrum of uranium dioxide observed experimentally and simulated theoretically following the procedure described above. The simulated spectra represent densities of oxygen 2p states convoluted with a 0.5 eV wide gaussian function.

observed and theoretically simulated electron energy loss spectra of NiO. It also illustrates the dependence of the equilibrium elastic properties of NiO on the choice of $\bar{U}$ and $\bar{J}$ entering the model Hamiltonian (1). The experimental energy loss spectra of NiO were obtained at the University of Cambridge, UK, using a dedicated scanning transmission electron microscope equipped with a Gatan Imaging Filter (UHV GIF model 678). The system uses a cold field emission gun and this facilitates the level of resolution of the order of 0.4–0.5 eV (as measured at the full width at half maximum of the zero loss peak). The near edge structure of the O K spectrum obtained in this way (the top row of graphs in Fig. 1) results from transitions from the occupied

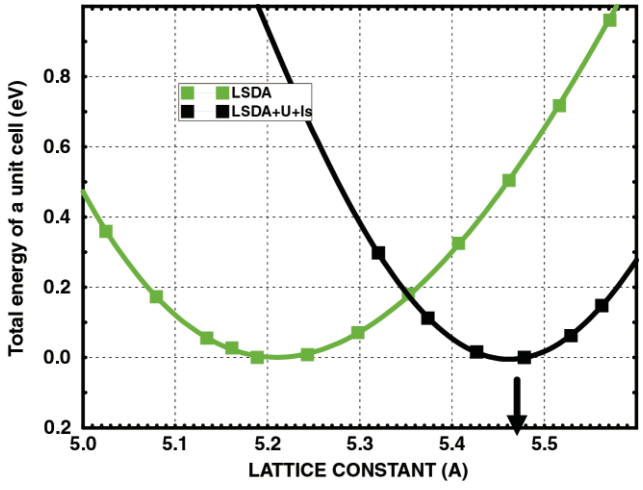

Fig. 4. Dependence of the total energy of a unit cell of uranium dioxide on the lattice constant. The experimentally observed value of the lattice constant equals 5.46 Å. The value of the bulk modulus determined using the curve shown on the right equals 2.02×10^{11} Pa and compares favourably with the experimentally observed value of 2.07×10^{11} Pa. The experimentally observed value of the equilibrium lattice constant is indicated by an arrow.

O 1s core levels to the conduction band states. Due to dominantly dipole selection rules and the necessary overlap of the initial and final states for the transition to be observed the final states probed are of p-symmetry and are localized on the oxygen sites.

Fig. 1 shows that as the value of $\bar{U}$ increases, the first peak in the EELS curve (peak A in the classification by Kanda et al., 1998) moves to the right and its intensity decreases. The origin of this effect can be explained in simple terms as resulting from the suppression of covalent bonding between oxygen 2p and nickel 3d states due to strong electron–electron correlations in the 3d shell. This conclusion also agrees with results of XANES calculations performed by Rez et al. (1995) for NiO clusters. Fig. 3 from the paper by Rez et al. (1995) shows that the first peak in the experimental EELS spectrum of NiO is shifted to the right in comparison with the position of the same peak predicted by LSDA calculations. LSDA calculations also have the tendency to overestimate the intensity of peak A in the simulated EELS spectra of NiO in agreement with results shown in Fig. 1.

Fig. 2 shows the partial densities of states of uranium dioxide calculated using DFT-LDA (where no Hubbard correction was included) and LSDA + U taking the spin–orbit interaction into account. Fig. 2 shows that in the case where the Hubbard correction term is not taken into account the Fermi level is situated in the lower part of the uranium 5f band giving rise to the prediction of a metallic ground state of this oxide. The LSDA + U calculations correctly describe UO_2 as an antiferromagnetic Mott–Hubbard insulator where the band gap of the order of 2.1 eV separates filled and empty parts of the uranium 5f band. Although the inclusion of spin–orbit interaction in the computational scheme (this interaction was not taken into account in our previous calculations, see Dudarev et al., 1997b) does not influence particularly strongly the distribution of the density of states shown in Fig. 2, by taking it into account it appears to be possible to eliminate the remaining degeneracy of f states and to improve the convergence of the method. If the spin–orbit coupling is not included in the computational scheme, the calculated size of the band gap turns out to be slightly smaller $E_g \sim 1.4$ eV (Dudarev et al., 1997b) than the experimental value of 2.1 eV. The inclusion of $(\mathbf{l}\cdot\mathbf{s})$ coupling also leads to the appearance of a non-zero orbital contribution to the magnetic moment localized on uranium ions. In the case of nickel oxide this additional contribution to the magnetic moment is small ($\sim 0.2\mu_B$ per ion), but in the case of uranium dioxide the orbital contribution to the magnetic moment is quite substantial: $\mu_L \sim -3.6\mu_B$. The total magnetic moment of a uranium ion is given by the difference $|\mu_L - \mu_S| \sim 1.7\mu_B$ which is very close to the experimentally observed value of $1.73\mu_B$.

Figs. 3 and 4 show, respectively, the experimentally observed and simulated EELS spectra of UO_2 and the dependence of the total energy of a unit cell of UO_2 evaluated using DFT-LDA and LSDA + U approaches.

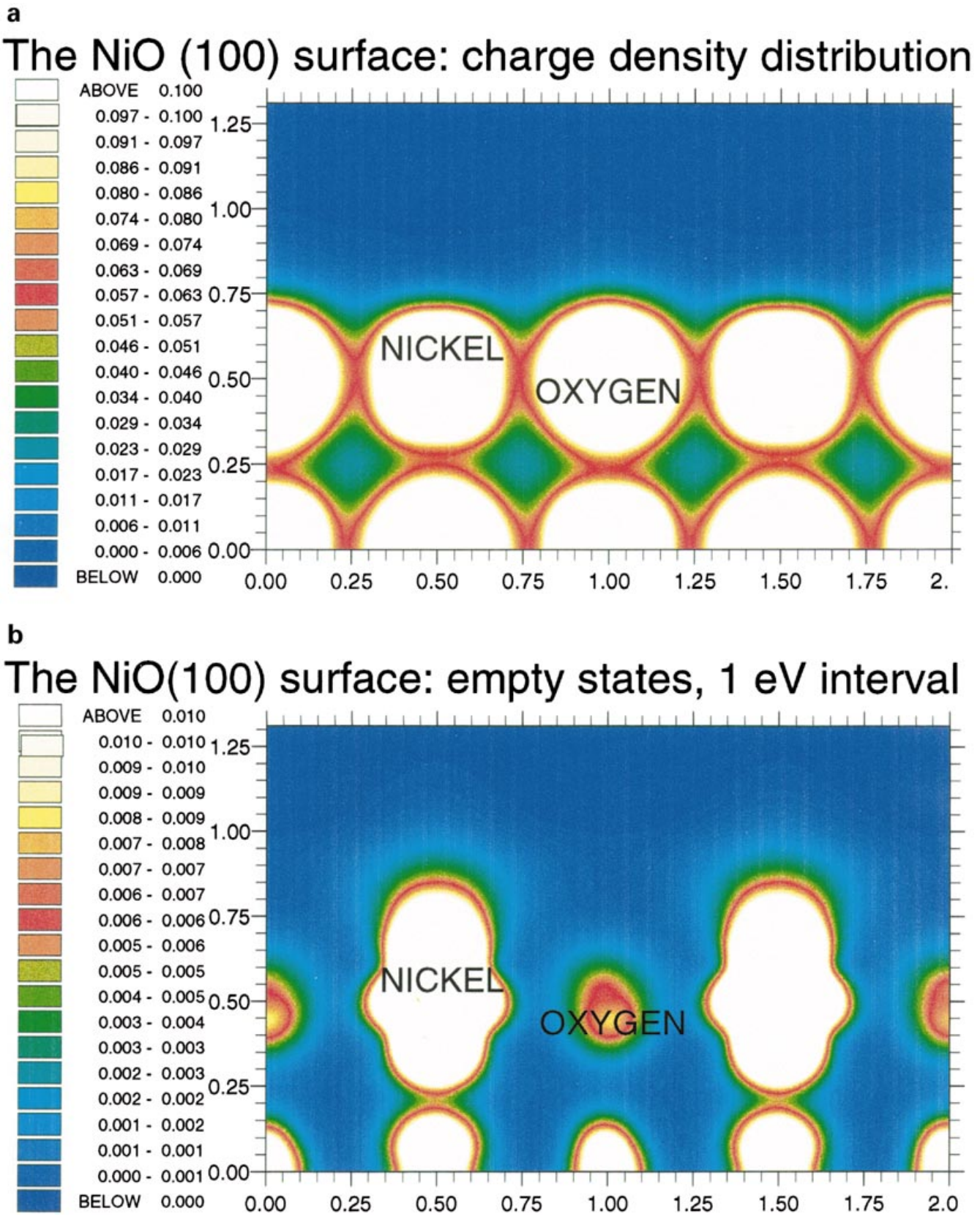

Fig. 5. Valence electron charge density distribution (a) calculated numerically for the NiO(001) antiferromagnetically ordered surface and the distribution of the density of *empty* states (b) calculated for the same surface by summing over a 1 eV interval corresponding to the bottom of the conduction band. Distances parallel and normal to the surface are expressed in units of the respective lattice constant.

The choice of $\bar{U} = 4.5$ eV leads to the best agreement between the data observed experimentally and simulated using ab initio methods. By comparing the experimental and simulated EELS spectra and also using information on the structural stability of NiO and UO_2 we have therefore determined values of parameters entering Hamiltonian (1) for these two oxides. In the next section we are going to use this information in order to interpret scanning tunnelling images of surfaces of NiO and UO_2.

4. Electronic states on NiO(001) and UO_2(111) surfaces and STM images

In the previous section we investigated how the value of Hubbard $\bar{U}$, which is the only adjustable parameter entering an LSDA + U electronic structure calculation, can be determined from the analysis of electron energy loss spectra. In what follows we are going to use values of $\bar{U}$ found above for NiO and UO_2 to investigate the *surface* electronic structure of the two oxides and to interpret experimental scanning tunnelling images of NiO(100) and UO_2(111) surfaces.

In the Bardeen approximation (Bardeen, 1961; Tersoff and Hamann, 1985) the tunnelling current is proportional to the square of the transition matrix element t_{TS} between electronic states Ψ_T and Ψ_S belonging to the tip and the sample. The magnitude of this matrix element is given by

$$t_{TS} = \frac{\hbar^2}{2m}\int_A \mathrm{d}\mathbf{A}\Big[\Psi_T(x,y,z_A(x,y))\frac{\partial}{\partial\mathbf{r}}\Psi_S^*(x,y,z_A(x,y)) - \Psi_S^*(x,y,z_A(x,y))\frac{\partial}{\partial\mathbf{r}}\Psi_T(x,y,z_A(x,y))\Big], \quad (4)$$

where the integration is performed over an arbitrary surface A separating the entire space into two parts, one including the tip and the other including the sample, in such a way that the effective one-electron potential vanishes everywhere at this surface. The tunnelling current is given by the Fermi golden rule as

$$I = \frac{2\pi}{\hbar}\sum_{S,T}(n_T - n_S)|t_{TS}|^2\delta(E_T - E_S), \quad (5)$$

where n_T and n_S are the occupation numbers of one-electron states of the tip and the sample, respectively. For a finite absolute temperature Θ these occupation numbers are given by

$$n_T = (\exp(E_T/k_B\Theta) + 1)^{-1} \qquad n_S = (\exp(E_S/k_B\Theta) + 1)^{-1}, \quad (6)$$

where the definition of E_T includes the shift associated with the applied bias. From Eqs. (4) and (5) it follows that the contrast of an STM image may be understood qualitatively in terms of the distribution of charge density in the vacuum region above the surface (see e.g. the analysis of STM images of TiO_2 performed by Diebold et al., 1996).

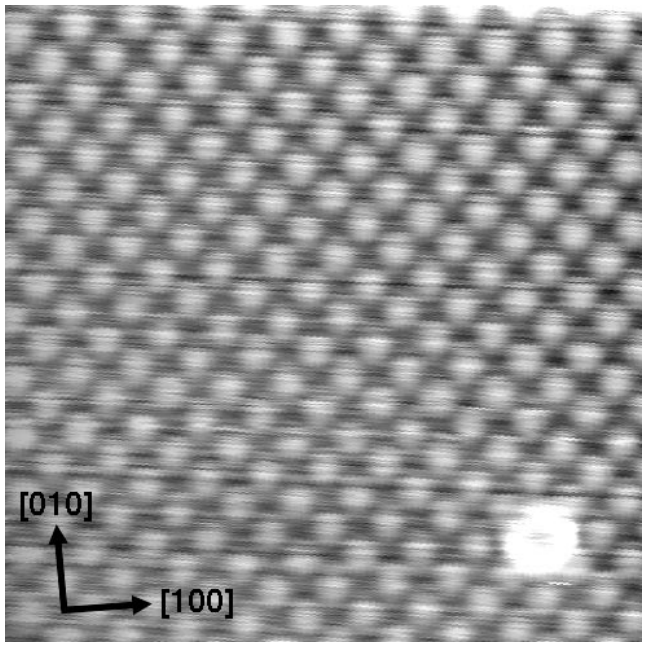

Fig. 6. Empty states STM image of NiO, ($V_{sample} = 1.3$ V, $I_{tunnel} = 1.0$ nA), (001) (1 × 1) UHV cleavage surfaces, where the bright dots show the Ni ions.

Calculations of the charge density distributions and distributions of *empty* electronic states integrated over a 1 eV interval of energies corresponding to the bottom of the conduction band were performed for antiferromagnetically ordered slabs of NiO and UO_2. For both cases, we used 18 k-points in the full (1 × 1) surface Brillouin zone and the same values of the Hubbard $\bar{U}$ and the exchange integral $\bar{J}$ as we obtained from the analysis of the total energy and EELS spectra describe above. It is likely that the value of $\bar{U}$ characterizing the strength of electron–electron repulsion in a localized shell of an ion situated at the surface should be expected to be larger than the value of $\bar{U}$ characterizing electron–electron interaction in the crystal bulk. However, given the insulating nature of both NiO and UO_2 it is reasonable to expect that the low mobility of carriers will give rise to practically the same degree of screening of the effective electron–electron interaction in the bulk as well as at the surface region of both oxides. This consideration justifies the use of 'bulk' values of $\bar{U}$ and $\bar{J}$ in surface electronic structure calculations.

Fig. 5(a) and (b) shows the charge density and empty state distributions calculated for the (001) unreconstructed and unrelaxed surface of NiO. Oxygen ions have larger radii and therefore the cross-section of the charge density distribution shown in Fig. 5(a) has peaks above oxygen sites. Nickel ions have 'flat' tops and do not stick far out into the vacuum region. At the same time, the real-space distribution of *empty* states shown in Fig. 5(b) is dominated by the nickel $3z^2–r^2$ d-states that protrude far into the vacuum

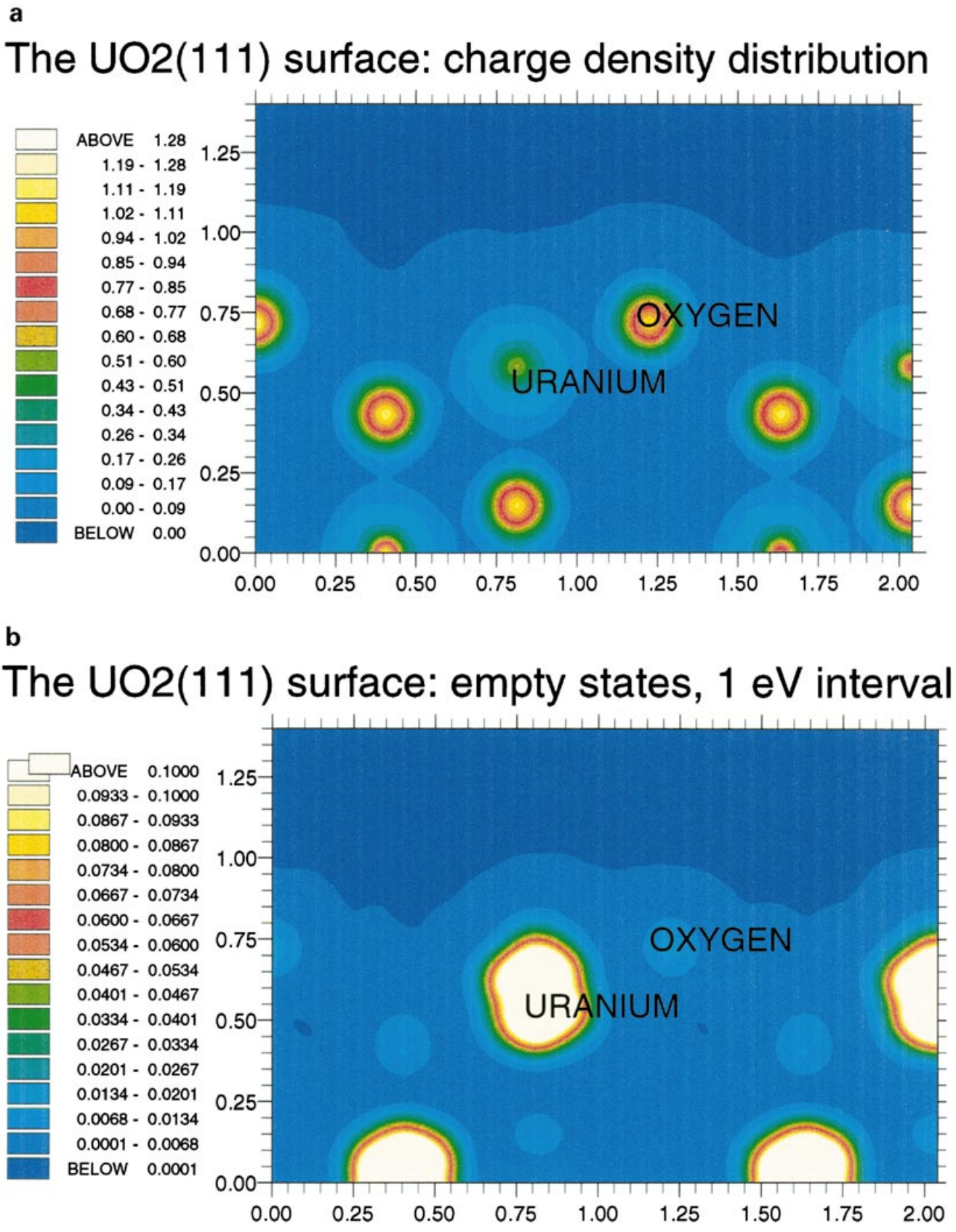

Fig. 7. Valence electron charge density distribution (a) calculated numerically for the UO_2(111) antiferromagnetically ordered surface and the distribution of the density of *empty* states (b) calculated for the same surface by summing over a 1 eV interval corresponding to the bottom of the conduction band. Distances parallel and normal to the surface are expressed in units of the respective lattice constant.

region and that are mainly responsible for tunnelling of electrons into the conduction band of the oxide at positive applied bias. The experimental STM image of the (001) surface of NiO shown in Fig. 6 was obtained using positive applied bias. By comparing Figs. 5 and 6 we can conclude that in images obtained using positive applied bias electrons tunnel predominantly into nickel 3d-states and it is therefore the nickel sublattice of NiO that is seen in Fig. 6.

A similar approach applied to the (111) surface of uranium dioxide shows that in this case the conclusions that can be derived from the comparison of experimental STM images and simulated charge density/empty state distributions are less straightforward. Fig. 7 (a) and (b) shows the charge density and empty state distributions calculated for the (111) unreconstructed and unrelaxed surface of UO_2. According to Fig. 7(a), the charge density near the UO_2(111) surface is peaked above oxygen ions while the empty states distribution (Fig. 7(b)) has maxima situated above uranium sites. This analysis seems to suggest that the surface lattice sites seen as bright in experimental STM images of UO_2 (one of these images is shown in Fig. 8) probably correspond to uranium ions. However, the difference in the position and in the height of the maxima of the distributions shown in Fig. 7(a) and (b) for UO_2(111) is significantly smaller than the difference in the shape of distributions shown in Fig. 5(a) and (b) which corresponds to the (001) surface of NiO. We therefore conclude that while in the case of NiO(001) the experimental STM images can be interpreted unambiguously on the basis of LSDA + U calculations described above, in the case of UO_2(111) further analysis is required in order to investigate the part played by the effects of surface reconstruction, surface–tip interactions and also by effects of strong electron–phonon coupling present in this oxide.

5. Summary

In this paper we described a new approach to modelling of electron energy loss spectra, equilibrium properties and scanning tunnelling images of surfaces of two metal oxides characterized by the presence of strong correlations between valence electrons. We showed that to describe the properties of NiO it was necessary to take into account the Hubbard correlations between 3d electrons of nickel ions. In the case of UO_2 a similar correction needs to be introduced in the description of the 5f uranium states. We have also shown how by combining information obtained using complementary experimental methods with results of first-principles theoretical calculations it has become possible to formulate a new approach to the characterization of surfaces of transition metal and actinide compounds.

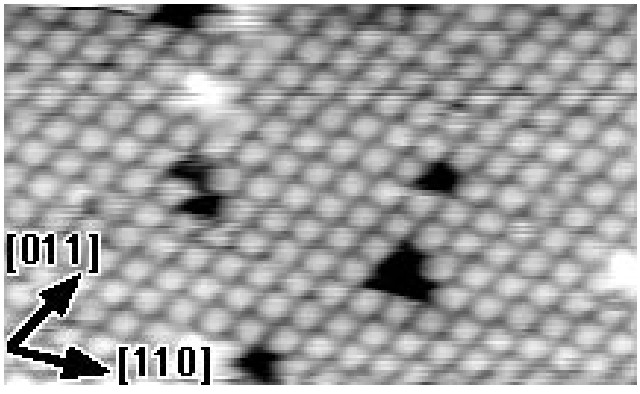

Fig. 8. Empty states STM image of UO_2, ($V_{sample} = 1.7$ V, $I_{tunnel} = 1.0$ nA), (111) (1 × 1) UHV cleavage surfaces, where the bright dots are believed to show the U ions.

Acknowledgements

S.L.D. would like to acknowledge financial support from Deutscher Akademischer Austauschdienst during his visit to Max-Planck-Institut für Festkörperforschung, Stuttgart. The authors would like to thank O.K. Andersen and D.G. Pettifor for stimulating discussions and we thank G. Thornton and P.L. Wincott for help with the NiO experimental STM work. Calculations were performed in the Materials Modelling Laboratory of the Department of Materials at the University of Oxford, UK, using an HP Exemplar V-class computer jointly funded by Hewlett–Packard and HEFCE through the JREI scheme. The work was also supported by BNFL and by the EPSRC JREI grant GR/M34454.

References

Adler, D., 1968. Insulating and metallic states in transition metal oxides. In: Seitz, F., Turnbull, D., Ehrenreich, H. (Eds.). Solid State Physics, 21. Academic Press, New York, pp. 1–113.

Anisimov, V.I., Zaanen, J., Andersen, O.K., 1991. Band theory and Mott insulators: Hubbard U instead of Stoner I. Physical Review B 44, 943–954.

Anisimov, V.I., Solovyev, I.V., Korotin, M.A., Czyzyk, M.T., Sawatzky, G.A., 1993. Density-functional theory and NiO photoemission spectra. Physical Review B 48, 16 929–16 934.

Anisimov, V.I., Aryasetiawan, F., Liechtenstein, A.I., 1997. First-principles calculations of the electronic structure and spectra of strongly correlated systems: the LDA + U method. Journal of Physics—Condensed Matter 9, 767–808.

Bardeen, J., 1961. Tunnelling from a many-particle point of view. Physical Review Letters 6, 57–59.

Brandow, B.H., 1977. Electronic structure of Mott insulators. Advances in Physics 26, 651–808.

Castell, M.R., Wincott, P.L., Condon, N.G., Muggelberg, C., Thornton, G., Dudarev, S.L., Sutton, A.P., Briggs, G.A.D., 1997. Atomic-resolution STM of a system with strongly correlated electrons: NiO(001) surface structure and defect sites. Physical Review B 55, 7859–7863.

Castell, M.R., Dudarev, S.L., Wincott, P.L., Condon, N.G., Muggelberg, C., Thornton, G., Nguyen-Manh, D., Sutton, A.P., Briggs, G.A.D., 1997. Atomic resolution STM of the NiO(001) surface structure and defect sites: $c(2 \times 2)$ patterning and effects of covalent bonding. Surface Review and Letters 4, 1003–1008.

Castell, M.R., Muggelberg, C., Dudarev, S.L., Sutton, A.P., Briggs, G.A.D.,

Goddard, D.T., 1998. Imaging insulating oxides by elevated temperature STM. Applied Physics A 66, S963–S967.

Castell, M.R., Dudarev, S.L., Muggelberg, C., Sutton, A.P., Briggs, G.A.D., Goddard, D.T., 1998. Surface structure and bonding in the strongly correlated metal oxides NiO and UO_2. Journal of Vacuum Science and Technology A 16 (3), 1055–1058.

Castell, M.R., Dudarev, S.L., Sutton, A.P., Briggs, G.A.D., 1999. Unexpected differences in the surface electronic structure of NiO and CoO observed by STM and explained by first principles theory. Physical Review B 59, 7342–7345.

De Boer, J.H., Verwey, E.J W., 1937. Semi-conductors with partially filled 3d-lattice bands. Proceedings of the Physical Society (London) 49, 59–71.

Diebold, U., Anderson, J.F., Ng, K.-O., Vanderbilt, D., 1996. Evidence for the tunnelling site on transition-metal oxides: TiO_2(110). Physical Review Letters 77, 1322–1325.

Dudarev, S.L., Liechtenstein, A.I., Castell, M.R., Briggs, G.A.D., Sutton, A.P., 1997. Surface states on NiO(001) and the origin of the contrast reversal in atomically resolved scanning tunnelling microscope images. Physical Review B 56, 4900–4908.

Dudarev, S.L., Nguyen-Manh, D., Sutton, A.P., 1997. Effect of Mott–Hubbard correlations on the electronic structure and structural stability of uranium dioxide. Philosophical Magazine B 75, 613–628.

Dudarev, S.L., Botton, G.A., Savrasov, S.Y., Humphreys, C.J., Sutton, A.P., 1998. Electron energy loss spectra and the structural stability of nickel oxide: an LSDA + U study. Physical Review B 57, 1505–1509.

Dudarev, S.L., Botton, G.A., Savrasov, S.Y., Szotek, Z., Temmerman, W.M., Sutton, A.P., 1998. Electronic structure and elastic properties of strongly correlated metal oxides from first principles: LSDA + U. SIC-LSDA and EELS study of UO_2 and NiO. Physica Status Solidi A 166, 429–443.

Dudarev, S.L., Castell, M.R., Briggs, G.A.D., Sutton, A.P., 1999. Bulk and surface electronic structure of NiO and CoO: a comparative ab initio LSDA + U analysis and application to the interpretation of STM images. Physica B 259/261, 717–718.

Ertl, G., Freund, H.-J., 1999. Catalysis and surface science. Physics Today (January), 32–38.

Fradkin, E., 1991. Field Theories of Condensed Matter Systems, Addison–Wesley, Reading, MA.

Freitag, A., Staemmler, V., Cappus, D., Ventrice, C.A., Al Shamery, K., Kuhlenbeck, H., Freund, H.-J., 1993. Electronic surface states of NiO(001). Chemical Physics Letters 210, 10–14.

Fulde, P., 1995. Electron Correlations in Molecules and Solids, 3. Springer, Berlin.

Gordon, M.J., Gaur, S., Kelkar, S., Baldwin, R.M., 1996. Low temperature incineration of mixed wastes using bulk metal oxide catalysts. Catalysis Today 28, 305–317.

Gorschlüter, A., Merz, H., 1994. Localized d–d excitations in NiO(001) and CoO(001). Physical Review B 49, 17 293–17 302.

Hutchins, G.J., Heneghan, C.S., Hudson, I.D., Taylor, S.H., 1996. Uranium-oxide based catalysts for the destruction of volatile. chloro-organic compounds. Nature 384, 341–343.

Hüfner, S., 1994. Electronic structure of NiO and related 3d-transition metal compounds. Advances in Physics 43, 183–356.

Kanda, H., Yoshiya, M., Oba, F., Ogasawara, K., Adachi, H., Tanaka, I., 1998. Cluster calculation of oxygen K-edge electron energy loss near edge structure of NiO. Physical Review B 58, 9693–9696.

Kiselev, V.F., Krylov, O.V., 1989. Adsorption and Catalysis on Transition Metals and Their Oxides, Springer, Berlin.

Kotani, A., Yamazaki, T., 1992. Systematic analysis of core photoemission spectra for actinide di-oxides and rare-earth sesqui-oxides. Progress in Theoretical Physics 108, 117–131.

Lichtenstein, A.I., Katsnelson, M.I., 1998. Ab-initio calculations of quasi-particle band structure in correlated systems: LDA++ approach. Physical Review B 57, 6884–6895.

Mott, N.F., 1974. Metal–Insulator Transitions, Taylor and Francis, London.

Muggelberg, C., 1997. The surface structures of uranium dioxide studied by elevated temperature STM. D.Phil. thesis, Wolfson College, Oxford.

Muggelberg, C., Castell, M.R., Briggs, G.A.D., Goddard, D.T., 1998. The atomic structure of the UO_2(111) surface and the effects of additional surface oxygen studied by elevated temperature STM. Surface Review Letters 5, 315–320.

Muggelberg, C., Castell, M.R., Briggs, G.A.D., Goddard, D.T., 1998. The atomic structure of the UO_{2+x}(110) surface and the effects of interstitial oxygen: an elevated-temperature STM study. Surface Science 402–404, 673–677.

Peierls, R., Mott, N.F., 1937. Discussion of the paper by De Boer and Verwey. Proceedings of the Physical Society (London) 49, 72–73.

Rez, P., Bruley, J., Brohan, P., Payne, M., Garvie, L.A.J., 1995. Review of methods for calculating near edge structure. Ultramicroscopy 59, 159–167.

Savrasov, S.Y., 1996. Linear-response theory and lattice dynamics: a muffin-tin-orbital approach. Physical Review B 54, 16 470–16 486.

Savrasov, S.Y., Savrasov, D.Y., 1992. Full-potential linear muffin-tin orbital method for calculating total energies and forces. Physical Review B 46, 12 181–12 195.

Spalek, J., 1990. Introduction: Mott insulators, correlated metals and high-temperature superconductors. Journal of Solid State Chemistry 88, 2–4.

Tersoff, J., Hamann, D.R., 1985. Theory of scanning tunnelling microscope. Physical Review B 31, 805–813.